Journal of Nuclear Materials 376 (2008) 152–159

Contents lists available at ScienceDirect

Journal of Nuclear Materials

journal homepage: www.elsevier.com/locate/jnucmat

Investigations of adsorption states of protium and deuterium in redeposited carbon flakes formed in tokamak T-10

N.Yu. Svechnikov [a,*], V.G. Stankevich [a], L.P. Sukhanov [a], K.A. Menshikov [a], A.M. Lebedev [a], B.N. Kolbasov [a], Y.V. Zubavichus [a], D. Rajarathnam [b]

[a] Russian Research Center Kurchatov Institute, Kurchatov Square, 1, Moscow 123182, Russia
[b] Department of Chemical and Biomolecular Engineering, 4 Engineering Drive 4, National University of Singapore, Singapore 117576, Singapore

ARTICLE INFO

Article history:
Received 2 August 2007

ABSTRACT

This work reports thermal desorption spectroscopy (TDS), Fourier-transform infrared (FT-IR) spectroscopy and X-ray diffraction (XRD) analyses on free standing redeposited hydrocarbon films (flakes) with a high deuterium to hydrogen isotopic ratio, produced in the T-10 tokamak in the Kurchatov Institute. XRD pattern showed that the carbon flakes differ substantially from graphite and are non-crystalline. The TDS $D_2(H_2)$ curves consist of two groups of peaks (450–800 K and 900–1000 K), and appeared to be rather similar to those obtained for a mechanically milled nanostructured graphite. As a result, two main adsorption states with activation energies of about 0.65 and 1.25 eV/H were found, implying a hopping diffusion and a resonance mechanism, respectively. The IR spectral differences between reddish-gold and dark-brown flakes showed a less degree of C–H hybridization for dark films and a disordered carbon network, to which the $CD_{2,3}$ end-groups are connected.

1. Introduction

Carbon materials eroded inside the vacuum chamber on plasma facing materials of the tokamak T-10 [1] and the other tokamaks (JET, Tore Supra, TEXTOR, DIII-D, TFTR [2]) during a deuterium (D) or deuterium–tritium (D–T) plasma discharge, redeposit inside the chamber in the form of carbon films and dust particles. Homogenous hydrocarbon films (reddish-gold, dark-brown flakes) were collected inside the tokamak vacuum chamber. The current study focuses mainly on reddish-gold flakes whose electronic and vibrational structures have been examined earlier by a number of techniques [1,3,4]. Unless regularly removed, these films with unlimited thickness may accumulate much deuterium and tritium, thus posing a severe problem for the International Thermonuclear Experimental Reactor (ITER) safety.

This work reports on thermal desorption spectroscopy (TDS), Fourier-transform infrared (FT-IR) spectroscopy and X-ray diffraction (XRD) analyses of free standing redeposited hydrocarbon reddish-gold (RG) and dark-brown (DB) flakes (20–30 μm thickness) having high atomic ratios of $D/C \approx 0.5$–0.6 (RG), $H/C \approx 0.1$–0.2 [4], produced in the T-10 tokamak operating in the Kurchatov Institute for one year campaign of 2002. The films have been formed under non-controllable conditions.

Though many reports are available on TDS studies of hydrogen isotopes obtained through graphite divertor tiles with deposited hydrocarbon films, hydrocarbon films formed from low temperature plasma discharges in laboratory devices, graphite and nanocarbon materials, wherein all samples were subjected to dosed adsorptions by neutral H(D) or ion $H^+(D^+)$ beams, no report of such studies on free standing hydrocarbon flakes formed inside tokamaks is available. Earlier IR studies with RG flakes [4] have shown the existence of two main deuterium vibrational states with different binding energies and stabilities. While the first one is characterized by the $CD_{2,3}$ sp^3 stretching modes at 2100–2200 cm^{-1} which appear with increasing deuterium concentration beyond $D/C \approx 0.2$, the other one is characterized by weak CD_2 sp^3 bending modes at 600–1100 cm^{-1}. The reported thermal desorption spectra (TDS) of flakes for H_2, HD and D_2 were also found to have two main groups of peaks, which correspond to two different adsorption states and mechanisms of their formation during the TD processes – resonance mechanism and hopping diffusion. The XRD data showed that the flakes' structure is almost amorphous, however, there seems to be a presence of structural elements (nanopores) in flakes with a typical size of about 1 nm. The latter is in agreement with theoretical estimation within the frame of hopping diffusion mechanism of hydrogen atoms along these structures.

2. Experiment

2.1. Samples

Carbon films under investigation were produced during the year 2002 experimental campaign [5] of the T-10 tokamak with

* Corresponding author. Fax: +7 8 499 196 7723.
E-mail address: svech1@km.ru (N.Yu. Svechnikov).

0022-3115/$ - see front matter © 2008 Elsevier B.V. All rights reserved.
doi:10.1016/j.jnucmat.2008.02.072

toroidal pump limiter configuration (RRC Kurchatov Institute). The main parameters of T-10 are the following: minor radius 0.39 m, major radius 1.5 m, minor radius of plasma 0.35 m, toroidal field 2.8 T, plasma current 200–400 kA, discharge time 1 s, electron temperature of core plasma – up to 1 keV, ion temperature 450–700 eV, additional heating power 1 MW. For regular and cleaning discharges the 99%D_2 + 1%H_2 gas mixture was used. Each experimental campaign started from vacuum vessel (VV) cleaning by heating up to 200 °C, inductive H_2 or D_2 discharges and He or Ar glow discharges. During experiments these procedures were repeated every night. The total duration of VV conditioning modes and plasma discharges in 2002 were the following: heating up to 200 °C – 897 h; inductive discharges – 35 h (H_2) and 270 h (99%D_2 + 1%H_2); He glow discharges – 86 h; D_2 plasma discharges – 1620 s.

During tokamak operation its plasma facing components, primarily local movable limiter contacting the plasma column from below and stationary annular diaphragm, made of a fine grain graphite MPG-8, are exposed to physical and chemical sputtering. Two types of C–D flakes and films were collected inside the T-10 tokamak vacuum chamber after chamber venting viz. homogeneous flakes and films (stratified), and flakes and films composed of globules (globular). There were also some films with intermediate structures. The homogeneous films used in this work were predominantly formed relatively far from the limiter and the diaphragm. The color differences of hydrogenated carbon films usually reflect the different hydrogen concentrations and different temperatures of film formation. The color of the homogeneous films strongly varies with D/C ratio, starting from dark-brown (DB), sometimes with soot particles on the plasma facing surface with atomic ratio D/C = 0.2−0.4, to semitransparent reddish-gold (RG) with D/C = 0.5–0.8, and to yellow with D/C > 1.0 [3]. Cracks and other defects on film surface lead to film flaking-off and cleavage, making it easier to be removed by scraper or vacuum cleaner. The films and flakes were formed on both shadowed and exposed to plasma surfaces. RG and yellow flakes were collected mainly in the shadowed areas, between two sidewalls forming the first wall where temperature was close to room temperature. DB flakes were collected on shadowed and exposed to plasma surfaces, relatively far from the limiter. Globular films were formed mainly near the limiter and diaphragm, in particular directly on the diaphragm surfaces. As for temperatures, due to short time of discharges and high heat capacity of structures, temperature of all the structures was close to room temperature. However because of high heat radiation during some discharges, surface temperature near the limiter was sometimes very high, e.g. basalt-fiber dust collector located on a movable rod within the discharge chamber nearby the limiter and the diaphragm, 225 mm away from the plasma column, was melted. The film thickness was measured with a profilometer. The Rutherford backscattering in combination with the resonance elastic scattering was used for analysis of deposits composition. Hydrogen isotopes depth profiles were measured with elastic recoil detection analysis by using He^+-ion beam with the energy of 1.9 MeV [4,5].

2.2. Methods

2.2.1. Fourier-transform infrared spectroscopy

The infrared reflectance spectra of flakes were obtained using a Bio-Rad IR-microscope (UMA-500) with a magnification of 500×, attached with a main frame multi-port Bio-Rad FT-IR spectrometer (FTS-3500), in retro-specular reflection mode. The main frame FT-IR consisted of a broad band Ge coated KBr beam splitter and the IR-microscope was equipped with a liquid nitrogen cooled high sensitive MCT detector with a scanning resolution of 8–10 μm. The spectra were obtained in the mid-IR range (4000–600 cm^{-1}) with a spectral resolution of 8 cm^{-1}, which covered the essential vibrational modes of C-, D-, H-, O-components of films. All the background measurements were done with a gold-coated mirror and the samples' absolute spectra were generated by Bio-Rad Win IR Pro 3.1 analytical software.

2.2.2. X-ray diffraction

Diffraction patterns of the carbon films were measured on an automated powder diffractometer DRON-3 (Cu Kα line λ = 154.18 pm). For the measurements, a single reddish-gold flake with an approximate size of 3 × 3 mm^2 was placed onto a glass sample holder. The diffraction contribution originating from the uncovered parts of the sample holder was subtracted from the experimental pattern after careful intensity normalization.

2.2.3. Thermal desorption spectroscopy

The experimental set-up for TDS experiments was based on a commercial UHV stainless-steel apparatus USU 4 (base pressure <1 × 10^{-9} mbar) equipped with an oil-free pumping system and a fast interlock for changing samples. TD spectra of flakes were taken by means of a commercial APDM-1 monopole mass-spectrometer (MS) (m/z = 1–200) in the temperature range 300–1070 K, under a constant heating rate dT/dt = 10 K/min. The flakes were encapsulated inside a small effusion stainless-steel (SS) Knudsen cell (∅6 × 20 mm^2) inserted into a ceramic tube with a heating tungsten winding. The orifice (∅2 mm) was directed towards the ionizer of the MS operating with electron beam energy of 100 eV in transversal ionization. The effusing flux passing through the MS ionizer was pumped off, without producing secondary particles by chemical reactions on the walls of the vacuum chamber. The latter was possible due to a spacing of 25 cm between ionizer and the walls of the chamber, while the distance between the Knudsen cell orifice and the ionizer was 2 cm. This construction resulted in a high sensitivity for TDS (<0.1 mg of flakes). The temperature was controlled by a W–Re thermocouple attached to the exit hole of the cell. Estimates of the temperature difference ΔT between the thermocouple and 2–3 pieces of flakes placed separately inside the Knudsen cell at T = 500 K, provided the flake heating occurred only due to thermal radiation according to the Stefan–Boltzmann law, gave the value of ΔT < 1 K for the given heating rate 10 K/min.

The average number of gas-wall elastic collisions inside a cell before escape of a gas molecule, estimated from the total cell surface to the orifice surface ratio, was about 140. This means, that the sticking coefficients of desorbing gases and hydrocarbon fragments on a SS surface must be smaller than 1/140 = 7 × 10^{-3}, in order to prevent possible adsorption of desorbing species and chemical reactions on the walls of the cell. The latter may include such processes on a transition metal surface of a cell, as a dissociative chemisorption due to C–H(D) bond breaking resulted from transfer of translational kinetic energy of desorbing fragments towards vibrational energy, when the latter helps to overcome a dissociation barrier [6], or a barrier for hydrocarbon coupling reactions [7]. Analysis showed that a possible minor adsorption of C-, CH-, C_2H-desorbing species or possible dissociative chemisorption of CH_4 on the SS walls of the cell at temperatures ≈600–700 K, cannot noticeably influence the TD spectra, in comparison with a usual TDS geometry without a Knudsen cell mass-spectrometry. The use of a Knudsen cell mass-spectrometry gave additional experimental possibilities, including a high TD spectral resolution by temperature (due to a low temperature gradient of the cell) and a high detection efficiency (due to a directional effusion of gas molecules from the cell).

The base vacuum before TDS experiments was about 3 × 10^{-9} mbar, and during heating the mass spectra background signals (m/z = 1–50) for an empty Knudsen cell during heating up to 1100 K were at least 2 orders of magnitude smaller than those

for flakes. The main efforts were aimed at registering simultaneous desorbing masses M2, M3 and M4, i.e. H_2, HD and D_2. However, the mass spectra signals M1–M50 were also taken during the flakes' heating in the temperature ranges 440–480 and 670–690 K, to estimate the desorption of hydrocarbons $C_xH_y(D_y)$ and water which may influence the H_2, HD and D_2 TD signals due to dissociative ionization under electron beam of ionizer.

3. Results and discussion

3.1. Infrared spectra of flakes

Fourier-transform infrared (FT-IR) reflectance spectra of reddish-gold (RG) and dark-brown (DB) flakes were obtained in the mid-IR region, 4000–600 cm^{-1}. Fig. 1 shows the combined spectra of two types of flakes. Fine spectral details are shown in Figs. 2–4.

As expected, the reflection signal from RG flakes is well pronounced due to better surface features. For the low-frequency region, 1700–600 cm^{-1} (Fig. 2), the difference, which may be due to concentration differences of adsorbates, is more visible. This implies that for RG flakes the surface has a much denser deposition of hydrocarbons leading to stronger (sharp) peak shapes compared to DB flakes. This is further evidenced from the line-shape of modes, which are wide and strongly hybridized for RG films, with the FWHM values of 10–40 cm^{-1}, compared to the FWHM values of 4–6 cm^{-1} for DB films.

The most of C–H vibrational modes in the region of 900–650 cm^{-1}, viz. 827, 782, 713, 671 cm^{-1} for RG films and 873, 861, 783, 753, 715 cm^{-1} for DB films correspond to out-of-plane deformational aromatic CH vibrations [8,9]. Some of these modes are hardly noticeable for DB films. The modes at 986, 894 (RG flakes) and 985 (DB flakes) are due to olefinic C–H out-of-plane bending vibrations [8,9]. The C–C skeletal stretching mode at 948 cm^{-1} **[10]** is observed only for RG flakes. The weak modes at 1098 (shoulder), 1087, 1058 and 661 cm^{-1} for RG films may be connected with bending CD_2 modes [10], whose intensities are 3–4 times weaker for DB flakes.

The wide RG mode at 1252 cm^{-1} corresponds to skeletal deformational vibration for the type $(CH_3)_3$–C– [8], which is scarce for dark films. The next weak and sharp modes at 1570, 1585 and 1595 cm^{-1} may be attributed to C=C aromatic ring skeletal stretching modes [8,9], and these modes are saturated for gold films. The weak features at 1711 and 1722 cm^{-1} are due to C=O stretching modes.

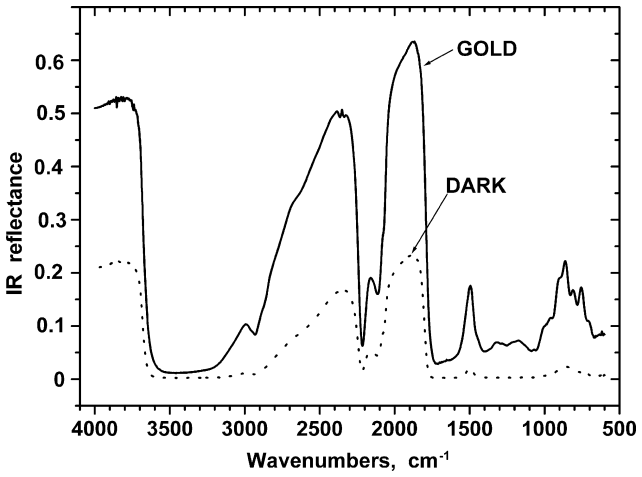

Fig. 1. Infrared reflectance spectra of reddish-gold and dark-brown flakes at RT in the mid-IR range.

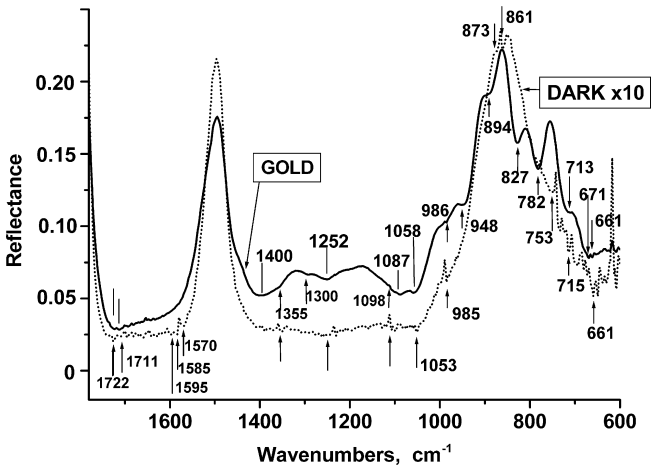

Fig. 2. The low-frequency part of the infrared spectra shown in Fig. 1 (the DB flake intensity is multiplied by 10).

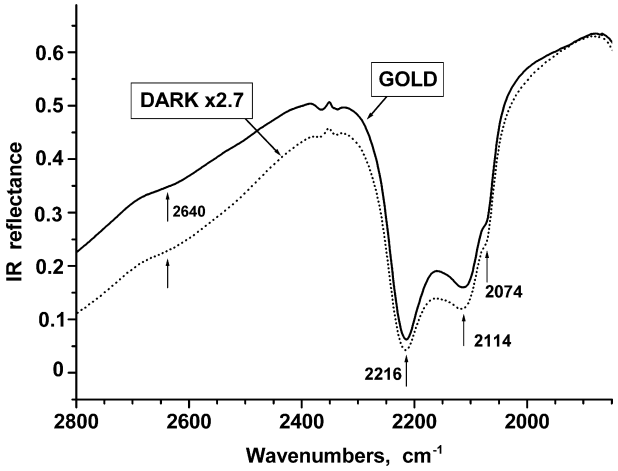

Fig. 3. Comparison of the stretching $CD_{2,3}$ modes of the infrared spectra shown in Fig. 1 (the dark film intensity is multiplied by 2.7).

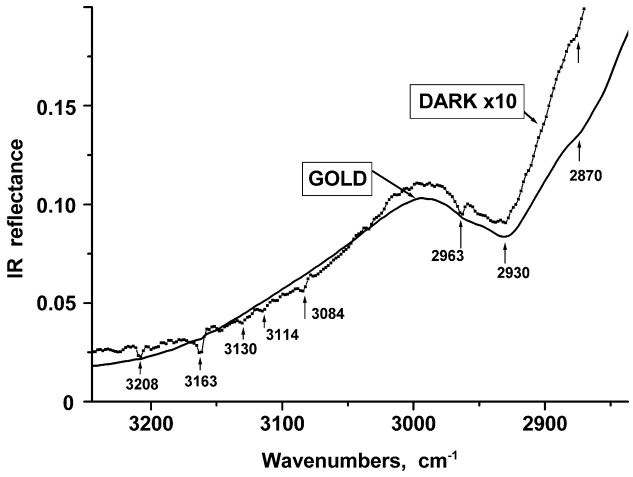

Fig. 4. The high-frequency part of the infrared spectra shown in Fig. 1 (the DB flake intensity is multiplied by 10).

For both types of flakes the most intense IR modes are observed for the C–D stretching modes at 2216 cm^{-1} (CD_3, asymmetric stretching), 2114 (CD_2, symmetric stretching) and 2074 (shoulder,

CD_3, symmetric stretching) shown in Fig. 3. Their absolute intensities differ by 2.7 times in favor of gold flakes, but the spectral shapes are very close, contrary to the case of C–C, C–H modes shown in Fig. 2. Both films possess a wide weak band centered at ≈2640 cm^{-1} (a shoulder) noticeable in Fig. 3, which is more evident for golden flakes. This feature may be attributed to the O–H stretching mode for systems containing a COOH group [8,9].

In the region 3300–2800 cm^{-1} (see Fig. 4) both films possess symmetric and asymmetric stretching CH_3 modes at 2870 (shoulder) and at 2963 cm^{-1}, respectively. A wide band at 2930 cm^{-1} is due to asymmetric CH_2 stretching mode. All these modes are saturated for gold films. There is a group of weak aromatic C–H stretching modes at 3084, 3114, 3130 and 3163 cm^{-1} resolvable only for dark flakes. The region of 3600–3200 cm^{-1} is known to be occupied mostly by stretched hydroxyl groups, namely, by at least two weak modes at 3208 (Fig. 4) and 3458 cm^{-1} (not shown) resolvable for dark flakes.

To summarize, the IR spectral difference between RG and DB flakes seems to be correlated with concentration differences of adsorbates and to the degree of C–H hybridization. Dark films have a more fragile and weak C–H interconnected adsorbates. The DB has less hydrogen adsorption which could be lead to much carbon – carbon network. Further, dark films seem to have more short carbon network structures with weak interconnections. The $CD_{2,3}$ stretching modes around 2200 cm^{-1} are nearly 2.7 times weaker for dark flakes and have an almost identical shape with those of gold flakes. For DB flakes these modes may not be introduced into the carbon net, but form the CD_2, CD_3 end-groups connected to the disordered carbon network.

3.2. XRD results

The X-ray diffraction pattern measured on one of the gold flakes reveals only a broad irregularly-shaped peak centered at about 10° (not shown). This implies that the sample is essentially non-crystalline. The profile of the peak can be deconvolved into 2 Gaussians at 11.5° and 31.8°, which correspond to the interplanar distances of 0.77 and 0.28 nm, respectively. The most intense line of graphite corresponds to the regular stacking of graphene layers observed at d_{002} = 0.335–0.345 nm, and the basic line corresponding to the in-plane hexagonal structure occurs at d_{100} = 0.214 nm. The diffraction patterns observed imply that the carbon flakes differ substantially from graphite and are essentially amorphous.

3.3. TD spectra

Fig. 5 shows experimental TDS curves for desorbed fluxes of hydrogen isotopes H_2, HD and D_2 from reddish-gold flakes at 300–1070 K. The TDS curves are complex, but in total these are composed of two main groups of peaks in the region 450–800 and 900–1000 K with comparable intensities and minima about 860 K. The peak shapes of H_2 and D_2 in the first group differ significantly, especially in the region of plateau at 540–620 K. With temperature growth the spectral shapes are becoming similar in the peak positions and structure. It is important to point out that the intensity of H_2 is higher than that for D_2 almost in whole region up to ≈770 K. Above this temperature the H_2 signal is becoming smaller than the D_2 one. In the second group of peaks it is to be noted that the shapes of H_2 and D_2 TD spectra near 970 K are similar indicating a possible common origin of both peaks, but the intensity of the D_2 peak is significantly higher than that for the H_2 one. Besides, the peak bandwidths in this region are narrower in comparison with the peaks of the first group.

The signal growth at 1100 K is connected with TD process, because this was absent during the heating of the empty Knudsen cell. Its origin may be connected with another adsorption states, which remained unresolved due to a limited power supply.

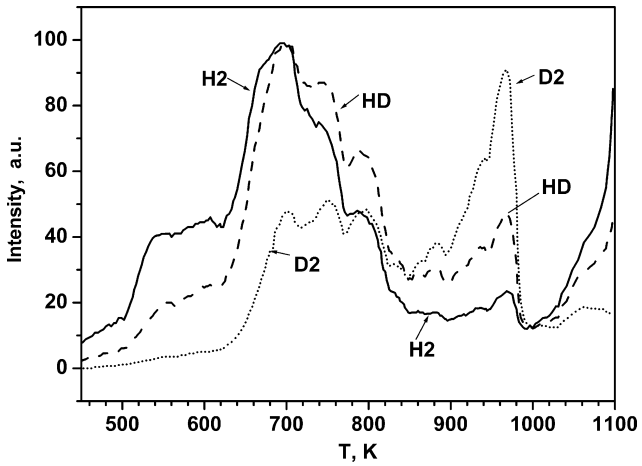

Fig. 5. TDS curves of H_2, D_2 and HD taken for reddish-gold flakes.

Note, that according to Janev and Reiter [11], there is no isotope effect in the direct and dissociative ionization channels, and the corresponding ionization cross sections are almost equal. Besides, the influence of transmission factors of QMS is known to be weakly mass dependent as $1/M^{3/8}$ for small masses [12]. Therefore, it is possible to compare the hydrogen TDS curves by intensities, and to estimate the influence of hydrocarbons' effusion (methane and higher) from flakes due to the known cross sections of electron impact direct and dissociative ionization [11,13–15], for H_2, D_2 signals and hydrocarbons. The analysis of the hydrocarbons' mass spectrum for M1–M50 (not shown) showed the dominant influence of the methane family on H_2, D_2 signals, among the other hydrocarbons. For example, the H_2 signal at 440–480 K contains ≈40% of H_2 and of D from the following channels of H_2^+ and D^+ production due to methane dissociative ionization in ionizer:

$$e + CH_4 \rightarrow H_2^+ + CH_2 + 2e, \quad e + CH_3 \rightarrow H_2^+ + CH + 2e,$$
$$e + CH_2 \rightarrow H_2^+ + C + 2e,$$
$$e + CD_4 \rightarrow D^+ + CD_3 + 2e, \quad e + CD_3 \rightarrow D^+ + CD_2 + 2e,$$
$$e + CD_2 \rightarrow D^+ + CD + 2e.$$

At 670–690 K this figure is reduced to 20%. The D_2 signal at 440–480 K contains almost 100% of deuterium from methane family, but at 660–700 K this value is about 20%.

Thus, the H_2 and D_2 signals are almost independent. Both H_2 and D_2 signals refer to HH (DD) recombination and desorption of the H_2 (D_2) molecules. At the same time, the HD curve is a result of such processes for H and D atoms in flakes. Therefore, the main attention was given to comparison of H_2 and D_2 TD curves. For comparison, in Fig. 6 are shown the H_2 and D_2 TDS curves of reddish-gold and dark-brown flakes. The first groups of low-temperature H_2 peaks have some differences in the range of 450–650 K, and are rather similar in the range of 650–850 K. The first group of D_2 peaks at 700–800 K has also some differences for both flakes. The high-temperature D_2 peak for the DB curve at 945 K coincides with the shoulder of the RG peak at 970 K, while the peak near 970 K is absent for dark flakes. Besides, the relative growth of the H_2 intensity at $T > 1000$ K is larger for the RG flakes. As a result, the whole TDS structure for both flakes cannot be regarded as totally different, i.e. their adsorption sites have similar features. The latter is most evident for high-temperature peaks (945–970 K), since these are less complex than the first wide group near ≈700 K.

The wide H_2 spectrum of flakes in Fig. 5 appeared to be rather similar in its initial part to that of *a*-C:H(D) films with a high H/C

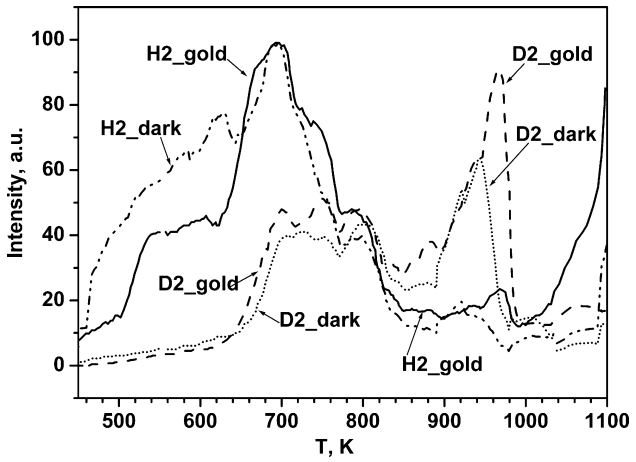

Fig. 6. Comparison of H_2 and D_2 TDS curves for reddish-gold and dark-brown flakes.

ratio about 0.5 from the work of Schenk et al. [16], where the H_2 desorption commences at 400 K, forms a plateau at 500–600 K, and a maximum near 720 K. These processes were explained by the surface origin [16,17].

The absence of a large shift between the H_2 and D_2 peak positions near 970 K in Fig. 5 indicates that the rate of hydrogen effusion may be limited by a detrapping process and not by diffusion [16], thus leading to a first order rate process.

The analysis of numerous spectra from publications on hydrogen TDS from different carbon materials shows that these features occur in the range of ≈400–1000 K (and higher) and have a large variety of spectral shapes. However, the shape and position of

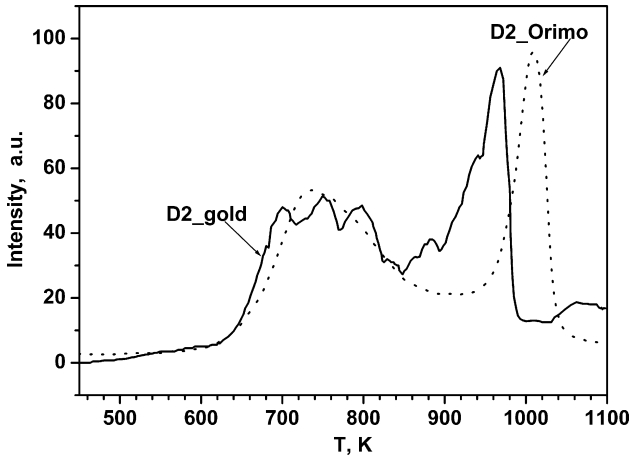

Fig. 7. Comparison of TDS curve for D_2 from Fig. 5 to D_2 curve taken from the work of Orimo et al. [18].

the TDS D_2 curve (Fig. 7) observed in the present study are comparable to those observed by Orimo et al. [18] for a nanostructured graphite (mechanically milled to <4 nm size under hydrogen atmosphere) under the same heating rate 10 K/min [19] as in our case. Two main groups of peaks are prominent with the first group of peaks centered near 750 K almost coinciding, while the second group of peaks near 1000 K is shifted by 40 K.

These spectral features imply the similarities in the states of hydrogen isotopes and TD processes within the given temperature range taking place in tokamak carbon flakes and nanostructured graphite. The structural similarity seems to be further evidenced through the XRD data which both reveal the absence of graphite-like diffraction peaks. Besides, our preliminary Raman spectra are also similar to those of Orimo et al. [18]. These spectral similarities allow the use of data already reported [18,19] on activation energies for interpretation of the present TD spectra.

Firstly, we shall try to explain the origin of peaks with a similar shape, located near the second desorption maximum at 970 K (Fig. 5), by means of the following model of H_2 (D_2) thermal desorption. During hydrogen adsorption on carbon dangling bonds, structural fragments with adjacent C–H bonds are formed, as shown in Fig. 8(a) for the case of sp^2 hybridization. During heating to ≈970 K two neighbor oscillating C–H bonds break, leading to a fast formation and a thermal desorption of a H_2 molecule Fig. 8(b). Consequently, two remaining dangling bonds recombine in step of a structural relaxation (Fig. 8(c)).

The mechanism of such type was proposed in a number of publications [20,21], for hydrogen desorption from pure sp^3 (*a*-Si, Si(100)) and sp^2 (graphite) systems, wherein the Si–H (or C–H) bond breaking occurs simultaneously with formation of a H_2 molecule, while two dangling bonds remain and then relax. The kinetic order for hydrogen desorption observed experimentally, was mainly the first order, since a H–H recombination is not a rate limiting step here. In the present case, the proposed mechanism is possible not only for sp^2 states (see Fig. 8(b)), but also for sp^3 states within the vibrating fragments $CH_{2,3}$ and $CD_{2,3}$. It is to be noted that for tokamak flakes [1], the nanostructure was found to be composed of two main phases: a diamond-like phase with C–H(D) sp^3 orbitals and σ-bonds, and a graphite-like phase with C–H sp^2 π-bonds, but almost no C–D sp^2 bonds were observable.

Within the frames of the proposed model, the isotope shift between activation energies of desorption for D_2 and H_2 is determined by the differences of zero point energies of participating molecular fragments, and it can be evaluated as follows:

$$\begin{aligned}\Delta E_a &= E_a(D_2) - E_a(H_2)\\ &= (1/2)\times\omega_e(H{-}H)\times\{[\omega_e(D{-}D)/\omega_e(H{-}H)]-1\}\\ &\quad -\omega_e(C{-}H)\times\{[\omega_e(C{-}D)/\omega_e(C{-}H)]-1\}.\end{aligned}\tag{1}$$

Since the ratios of vibrational frequencies for the hydrogen–hydrogen and carbon–hydrogen bonds are almost equal, then

$$\omega_e(D{-}D)/\omega_e(H{-}H) = 1/\sqrt{2} \approx \omega_e(C{-}D)/\omega_e(C{-}H)\tag{2}$$

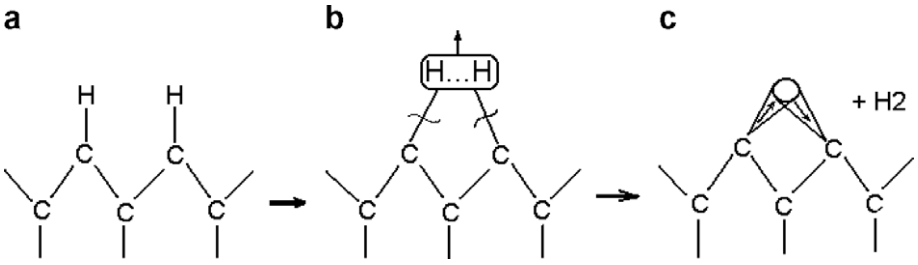

Fig. 8. (a–c) Mechanism of molecular thermal desorption for TDS peaks near 970 K, corresponding to the case of sp^2 hybridization (see the text).

and the isotope shift is given by

$$\Delta E_a \approx 0.293 \times [\omega_e(\mathrm{C{-}H}) - (1/2) \times \omega_e(\mathrm{H{-}H})]. \quad (3)$$

On the other hand, the isotope shift can be evaluated from the small TD spectral shift for D_2 and H_2 maxima near $T_m = 970$ K (Fig. 6), reaching the value of $\Delta T_m \approx 3$ K. In linear approximation of a small parameter $\Delta T_m/T_m \ll 1$, it follows:

$$\Delta E_a \approx E_a \times (\Delta T_m/T_m) = 62\ \mathrm{cm}^{-1}, \quad (4)$$

for $E_a = 2.5$ eV/H_2 [18]. Comparing Eqs. (3) and (4), we obtain

$$\omega_e(\mathrm{C{-}H}) - (1/2) \times \omega_e(\mathrm{H{-}H}) \approx 212\ \mathrm{cm}^{-1}. \quad (5)$$

From (5) it follows that for the standard vibrational frequency of the H_2 molecule, $\omega_e(\mathrm{H{-}H}) = 4401\ \mathrm{cm}^{-1}$ [22], the vibrational frequency of the C–H bonds during the TD process should reach the value of $\omega_e(\mathrm{C{-}H}) \approx 2413\ \mathrm{cm}^{-1}$, which is smaller than the above mentioned stretching vibrational modes about 2900 cm^{-1} and higher than the deformational modes in the region of ≈1400–1500 cm^{-1}, or aromatic C–H modes at 700–900 cm^{-1}. Thus, the vibrational energy of two neighbor C–H bonds will be quite sufficient for effective participation in the molecular desorption (Fig. 8(b)). The same is true for deuterium desorption, where $\omega_e(\mathrm{C{-}D}) \approx 1706\ \mathrm{cm}^{-1}$ (see the ratio (2)), and this is smaller than the above mentioned stretching vibrational modes about 2200–2100 cm^{-1}.

The proposed model of molecular desorption stems from the rupture of the existing chemical bonds (eased by C–H, C–D vibrations) and formation of new chemical bonds, thus describing the observable resonance-type process. This peculiarity of molecular desorption is manifested in an ensemble of narrow TD peaks around 970 K, in comparison with a group of wide peaks near $T_m \sim 700$ K (see Fig. 5). Moreover, the proposed model corresponds to the first order kinetics leading to an asymmetrical shape of TDS peak near the maximum (see, e.g. [23]), which seems to be the case for the observable peaks near $T_m = 970$ K.

The wide TD peak observed by Atsumi et al. [19] for nanostructured graphite, whose shape and position are similar to those of wide peaks observed in the present study near 700 K, can be explained by molecular H_2 diffusion through the nanopores with an activation energy of diffusion $E_a = 1.3$ eV/H_2. The origin of low-temperature peaks may be explained by the mechanism of hopping diffusion of hydrogen along defect sites.

It is considered that the diffusing molecule (or atom) is hopping between two equivalent potential wells with the barrier height U_a (see Fig. 9) and spaced at the distance λ. The potential relief is approximated by similar parabolas (and inverted parabolas) with a curvature coefficient k with both signs. Parabolas are smoothly connected in the middle of the barrier height, i.e. $U(x) = U_a/2$ at distances $x = \lambda/4$ and $3\lambda/4$, and one will obtain the following ratios:

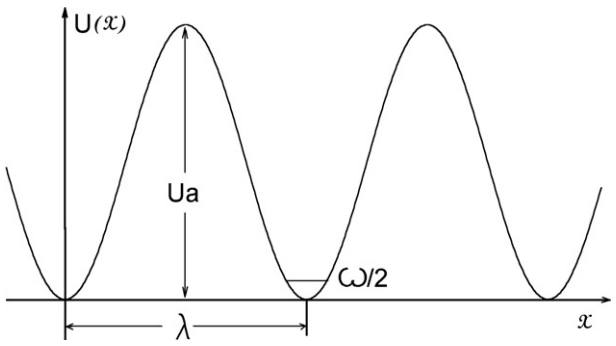

Fig. 9. Potential energy diagram of hydrogen hopping diffusion for the TDS wide group near 700 K.

$$k = 16U_a/\lambda^2 = m\omega^2, \quad (6)$$

$$\lambda = 4(U_a/k)^{1/2} = (4/\omega)(U_a/m)^{1/2}. \quad (7)$$

Here ω is a vibrational frequency of a particle with a mass m within a potential well. It is to be noted that the hopping distance λ is independent of isotope mass m, as seen from the left side of the formulas (7). The activation energy for diffusion E_a is connected with the potential barrier height U_a

$$U_a = E_a + \omega/2. \quad (8)$$

In the case of hydrogen molecule transport, the isotope shift in the activation energy for diffusion of H_2 and D_2, taking into account the ratio (2), is equal to

$$\Delta E_a(H_2) = E_a(D_2) - E_a(H_2) = (1/2)\omega(H_2)[1 - \omega(D_2)/\omega(H_2)] \approx 0.147\omega(H_2). \quad (9)$$

From formulae (4) and (9), the isotope shift $\Delta T_m \approx 6$ K taken from our TD spectra near 700 K, and assuming $E_a = 1.3$ eV/H_2 [19], the vibrational frequency of a H_2 molecule in the potential well can be evaluated before desorption as follows:

$$\omega(H_2) \approx (1/0.147)E_a(\Delta T_m/T_m) \approx 0.076\mathrm{eV} = 616\ \mathrm{cm}^{-1} = 1.8 \times 10^{13}\ \mathrm{s}^{-1}. \quad (10)$$

According to the ratio (8), when $U_a \approx E_a = 1.3$ eV/H_2 the H_2 hopping distance from (7) reaches to λ (H_2) = 1.72 nm.

It is important to note that the mechanism of molecular $H_2(D_2)$ diffusion [19,24–26] suggests the presence of a H_2 molecule in the bulk of carbon materials under normal conditions as a result of physisorption in nanopores. This process is characteristic for certain types of graphite and carbon nanotubes and is observable in the $H_2(D_2)$ Raman spectra at low- temperatures and high pressures [27]. However, neither the present Raman and IR experimental data, nor the known literature data on Tokamak flakes show the signs of the H_2 presence in the bulk of flakes. Thus it is reasonable to consider the model of atomic H(D) transport in flakes, followed by a fast atomic recombination near common defect, as proposed by Haasz et al. [28].

In the context of the hopping diffusion mechanism, the isotope shift for the activation energies of H(D) atomic diffusion is equal to

$$\Delta E_a(H) = E_a(D) - E_a(H) = (1/2)\omega(H)[1 - \omega(D)/\omega(H)] \approx 0.147\omega(H). \quad (11)$$

According to Atsumi et al. [19], the activation energy was decreased by 2 times to a value of $E_a = 0.65$ eV/H, which implies that from the ratio (10) the vibrational frequency of an H atom in the potential well can be given as: $\omega(H) = \omega(H_2)/2 = 0.038$ eV = 308 cm^{-1} = $0.9 \times 10^{13}\ \mathrm{s}^{-1}$. The obtained frequency $\omega(H) = 308\ \mathrm{cm}^{-1}$ corresponds to a physisorption of a hydrogen atom, which is in contrast to the above mentioned mechanism of resonance exchange of chemical bonds during H_2 desorption near 970 K. In the far IR region below 600 cm^{-1}, only the experimental deformational carbon – deuterium mode at 295 cm^{-1} is observable [29]. The situation may be connected with the presence of some portion of unbound hydrogen (or weakly bound in interstitials or occluded), which is not observed in IR spectra. This is well known for polymeric *a*-C:H(D) films [30], where this H unbound quantity may reach up to 50%. Possibly, the ratio of unbound hydrogen is higher for dark flakes, having a more disordered structure of a carbon network.

According to the ratio (8), when $U_a \approx E_a = 0.65$ eV/H, the H hopping distance from the ratio (7) becomes $\lambda(H) = 2\ \lambda(H_2) = 3.44$ nm. Taking into account our XRD assumptions on the presence of

structural elements (nanopores) in flakes with a typical size of a few nm, the wide TDS group of peaks near 700 K (Fig. 5) may be related to H(D) atomic hopping between such elements, followed by a fast pair recombination on one of them.

The prefactor in the atomic diffusion coefficient can be evaluated as: $D_H \sim \omega(H) \times \lambda_H^2 = 1.09 \times 10^{-4} m^2/s$, which is rather close to the corresponding value of 1.48×10^{-4} m^2/s reported by Haasz et al. [28] for atomic diffusion along the crystallite surfaces in graphite. The diffusion activation energy, E_a = 0.65 eV/H, calculated in the present study is also rather close to the corresponding activation energy for surface diffusion of 0.56 eV/H, taken from the experimental data by Haasz et al. [28].

This is contrary to the obtained prefactor values of 3.3×10^{-10} m^2/s and 3.8×10^{-13} m^2/s for molecular bulk diffusion of hydrogen in graphite [24] and molecular bulk diffusion in micropores of graphite [25], respectively.

These comparisons suggest that hydrogen diffusion in the region of the low-temperature desorption peaks occurs by means of a hopping diffusion of physisorbed hydrogen atoms, followed by their subsequent fast recombination near a common structural element. The high-temperature peak at 970 K is related to a resonance-type process, i.e. simultaneous desorption and recombination of chemisorbed hydrogen isotopes.

It is of interest to correlate the formation conditions of flakes inside tokamak T-10 and the observed two groups of TD peaks. The similarity of the low-temperature group (450–800 K) between TD spectra of flakes and those for *a*-C:H(D) films [16] suggests that formation conditions are the same. Therefore, the first group of peaks may be influenced by glow discharges used during the VV T-10 cleaning. Moreover, despite of using the 99%D_2 + 1%H_2 gas mixture discharge that would lead to a high D_2/H_2 ratio, the origin of a large H_2 signal in this spectral region is not yet clear.

Indeed, according to the working cycles of tokamak T-10 mentioned in Section 2.1, the main origin of hydrogen adsorption could be the heating (200 °C, 897 h) and inductive H_2 glow discharges (35 h), contrary to inductive D_2 discharges (270 h) and D_2 plasma discharges (1620 s). However, this quantity of hydrogen would be insufficient for the observable ratio for integrals under the TD curves in Figs. 5 and 6: $H_2/D_2 \approx 1.5$ (golden flakes) and 1.9 (dark flakes). Also, this can be explained by deuterium substitution of hydrogen on the surface as was proposed by Masaki et al. [31]. The effective release and removal of hydrogen isotopes and carbon during He glow discharge cleaning was noted by Kobayashi et al. [32], while the amount of hydrocarbons was much larger during tokamak discharges.

Also, the uptake of a water vapor from atmosphere during the VV venting with a subsequent dissociation of water to $H^+ + OH^-$ during tokamak operations may take place. The high intensity mass-spectrometry signals with m/z = 17–18 seem to confirm the presence of water in flakes, though these signals refer both water and methane fragments, i.e. $OH + CD_2H$ and $H_2O + CD_3$, respectively.

The similar puzzling problem of a high H_2/D_2 ratio >2–5, i.e. an order of magnitude higher than the ratio of the respective number of discharges performed with hydrogen and deuterium, was discussed in the work on tokamak flakes adsorbed on graphite tiles [33,34]. The H_2 TDS shoulder at 500–600 K [33] was partly attributed to water from atmosphere, however, the second heating of samples showed the similar spectral shape in this region. Moreover, such a shoulder was also observed for *a*-C:H(D) films with a high H/C ratio about 0.5 investigated *in situ* by Schenk et al. [16]. These observations lead to an ambiguity to arrive at a conclusion.

On the other hand, the high-temperature TD group (900–1000 K) in Fig. 5 correlates with conditions of regular and cleaning discharges of the 99%D_2 + 1%H_2 gas mixture of tokamak T-10, leading to a high D_2/H_2 ratio.

4. Conclusions

Analytical techniques of FT-IR, XRD and TDS with Knudsen cell mass-spectrometry were performed on free standing redeposited hydrocarbon reddish-gold and dark-brown films (flakes) from tokamak T-10, having high D/C and H/C ratios. Analysis of the data enabled to arrive at following details:

(1) The TDS curves for $D_2(H_2)$ consist of two groups of peaks, 450–800 K and 900–1000 K, and appeared to be rather similar to those already reported [18] for a nanostructured graphite mechanically milled to the <4 nm size under the same heating rate. This TDS resemblance together with similarities in XRD and Raman spectra, shows the similarities in the TD processes. Therefore, the reported data on activation energies were used for interpretation of TD spectra of present work.

(2) Two main adsorption states of hydrogen isotopes were revealed: a weak physisorbed state with a binding energy ≈0.65 eV/H and a strong chemisorbed one with a binding energy ≈1.25 eV/H. The whole TDS structure of gold and dark flakes cannot be regarded as totally different, i.e. their adsorption sites have similar features. Two desorption mechanisms were suggested: a hopping diffusion mechanism for H(D) atomic hopping between weakly bonded states on structural elements (nanopores), followed by a fast pair recombination on one of them, and a resonance mechanism for strongly bonded states.

(3) The IR spectral differences between golden and dark flakes seem to be correlated well with concentration differences of carbon deposits and to the degree of C–H hybridization. The dark flakes have less hydrogen adsorption which could be lead to much carbon–carbon network. Dark films have a more fragile and weak C–H interconnected adsorbates, more short carbon network structures. The $CD_{2,3}$ stretching modes around 2200 cm^{-1} are weaker for dark flakes, and these modes need not be introduced into the carbon net, but form the CD_2, CD_3 end-groups connected to the disordered carbon network.

Acknowledgements

The authors would like to thank Dr L.N. Khimchenko for supplying samples, and Dr K.Yu. Vukolov for fruitful discussions.

References

[1] N.Yu. Svechnikov, V.G. Stankevich, A.M. Lebedev, K.A. Menshikov, B.N. Kolbasov, M.I. Guseva, L.N. Khimchenko, D. Rajarathnam, Yu.Yu. Kostetsky, Plasma Dev. Oper. 14 (2) (2006) 137.
[2] G. Federici, Ch.H. Skinner, J.N. Brooks, J.P. Coad, Ch. Grisolia, A.A. Haasz, A. Hassanein, V. Philipps, C.S. Pitcher, J. Roth, W.R. Wampler, D.G. Whyte, Plasma-material interactions in current tokamaks and their implications for next-step fusion reactors, A joint report with the Princeton Plasma Physics Laboratory (Princeton, NJ, USA) and the Max-Planck-Institut fur Plasmaphysik (Garching, Germany), PPPL-3531, IPP-9/128, 2001.
[3] B.N. Kolbasov, P.V. Romanov, M.I. Guseva, B.I. Khripunov, V.G. Stankevich, N.Yu. Svechnikov, A.M. Zimin, Plasma Dev. Oper. 14 (4) (2006) 303.
[4] N.Yu. Svechnikov, V.G. Stankevich, A.M. Lebedev, K.A. Menshikov, B.N. Kolbasov, M.I. Guseva, K.Yu. Vukolov, D. Rajarathnam, N.M. Kocherginsky, Yu. Kostetski, Fus. Eng. Design 75–59 (2005) 339.
[5] K.Yu. Vukolov, V.M. Gureev, M.I. Guseva, L.S. Danelyan, S.A. Evstigneev, S.N. Zvonkov, in: Proceedings of the 31st EPS Conference on Plasma Physics, London, UK, 28 June–2 July 2004, ECA vol. 28G, P.1-184, 2004, P4.
[6] R. Milot, A.P.J. Jansen, Phys. Rev. B 61 (23) (2000) 15657.
[7] M. Neurock, D. Walthall, An *ab initio* approach towards engineering Fischer-Tropschsurface chemistry, Technical Progress Report, 2006, p. 1. <http://www.osti.gov/bridge/servlets/purl/882888-OhxbyH/882888.PDF>.
[8] L.J. Bellamy, Infrared Spectra of Complex Molecules, third ed., 1975.
[9] John Coates, in: R.A. Meyers (Ed.), Encyclopedia of Analytical Chemistry, John Wiley & Sons Ltd., Chichester, 2000, p. 10815.

[10] D. Blaudez, T. Buffeteau, N. Castaings, B. Desbat, J.-M. Turlet, J. Chem. Phys. 104 (24) (1996) 9983.
[11] R.K. Janev, D. Reiter, Collision processes of hydrocarbon species in hydrogen plasmas: 1. The methane family, Report FZ-Jülich Jül-3966. <http://www.eirene.de/html/a_m_data.html>.
[12] G.I. Slobodeniuk (Quadrupole Mass-spectrometers), Atomizdat, Moscow, 1974. p. 272 (in Russian).
[13] R.K. Janev, D. Reiter, Collision processes of hydrocarbon species in hydrogen plasma: 2. The ethane and propane families, Report FZ-Jülich Jül-4005. <http://www.eirene.de/html/a_m_data.html>.
[14] Cechan Tian, C.R. Vidal, J. Phys. B 31 (1998) 895.
[15] V. Tarnovsky, A. Levin, H. Deutsch, K. Becker, J. Phys. B 29 (1996) 139.
[16] A. Schenk, B. Winter, J. Biener, C. Lutterloh, U.A. Schubert, J. Küppers, J. Appl. Phys. 77 (6) (1995) 2462.
[17] Ch. Wild, P. Koidl, Appl. Phys. Lett. 51 (19) (1987) 1506.
[18] S. Orimo, T. Matsushima, H. Fujii, T. Fukunada, G. Majer, J. Appl. Phys. 90 (3) (2001) 1545.
[19] H. Atsumi, K. Tauchi, J. Alloys Compd. 356–357 (2003) 705.
[20] J. Farjas, D. Das, J. Fort, P. Roura, E. Bertran, Phys. Rev. B 65 (2002) 115403.
[21] U. Höfer, Leping Li, T.F. Heinz, Phys. Rev. B 45 (16) (1992) 9485.
[22] K.P. Huber, G. Herzberg, Molecular Spectra and Molecular Structure. IV. Constants of Diatomic Molecules, Van Nostrand Reinhold Company, New-York, 1979.
[23] D.P. Woodruff, T.A. Delchar, Modern Techniques of Surface Science, Cambridge University, Cambridge, London, New-York, New Rochelle, Melbourne, Sydney, 1986. 568p., p. 360.
[24] H. Atsumi, J. Nucl. Mater. 307–311 (2002) 1466.
[25] I.E. Gabis, Phys. Technol. Semicond. 31 (2) (1997) 145 (in Russian).
[26] E.A. Denisov, T.N. Kompaniets, J. Technol. Phys. 71 (2) (2001) 111 (in Russian).
[27] K.A. Williams, B.K. Pradhan, P.C. Eklund, M.K. Kostov, M.W. Cole, Phys. Rev. Lett. 88 (16) (2002) 165502.
[28] A.A. Haasz, P. Franzen, J.W. Davis, S. Chiu, C.S. Pitcher, J. Appl. Phys. 77 (1) (1995) 66.
[29] H. Okuyama, H.S. Kato, M. Kawai, RIKEN Rev. 37 (2001) 24.
[30] .A. Grilll, V. Patel, Appl. Phys. Lett. 60 (17) (1992) 2089.
[31] K. Masaki, T. Tanabe, Y. Hirohata, Y. Oya, T. Shibahara, T. Hayashi, K. Sugiyama, T. Arai, K. Okuno, N. Miya, Nucl. Fus. 47 (11) (2007) 1517.
[32] Y. Kobayashi, K. Isobe, A. Kaminaga, H. Nakamura, K. Tsuzuki, S. Higashijima, S. Konishi, Analysis of Exhaust Gas in JT-60U Tokamak Operation, Twenty-First IEEE/NPSS Symposium on Fusion Engineering 2005. <http://www.telegrid.enea.it/Conferenze/SOFE05/DATA/08_04.PDF>.
[33] P. Franzen, R. Behrisch, C. Garcia-Rosales, et al., Nucl. Fus. 37 (10) (1997) 1375.
[34] Y. Hirohata, T. Tanabe, Y. Oya, K. Shibahara, T. Arai, et al., in: M. Matsuyama, Y. Hatano (Eds.), The 3-d International Workshop on Tritium-material interactions, May 20–21 2005, Toyama, Japan (Satellite meeting of the 7-th ISFNT).